Figure 1: Detection of AGR2 specificity by ELISA

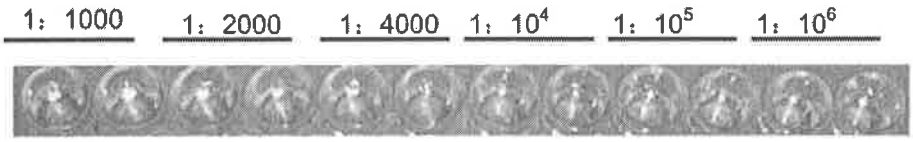


Figure 2: Detection of AGR2 specificity by immunoblotting

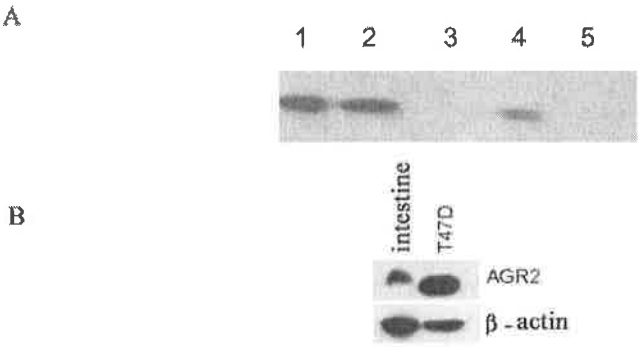


Figure 3: Detection of AGR2 specificity by immunoprecipitation

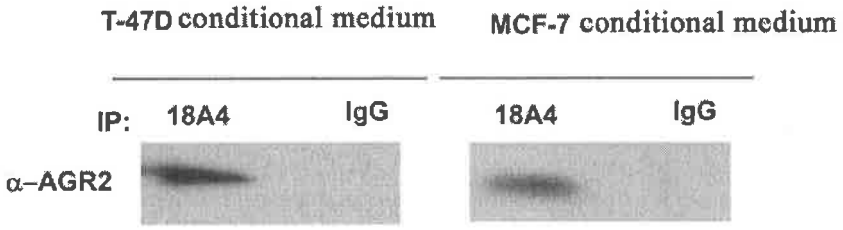


Figure 4: Detection of AGR2 specificity by immunofluorescence

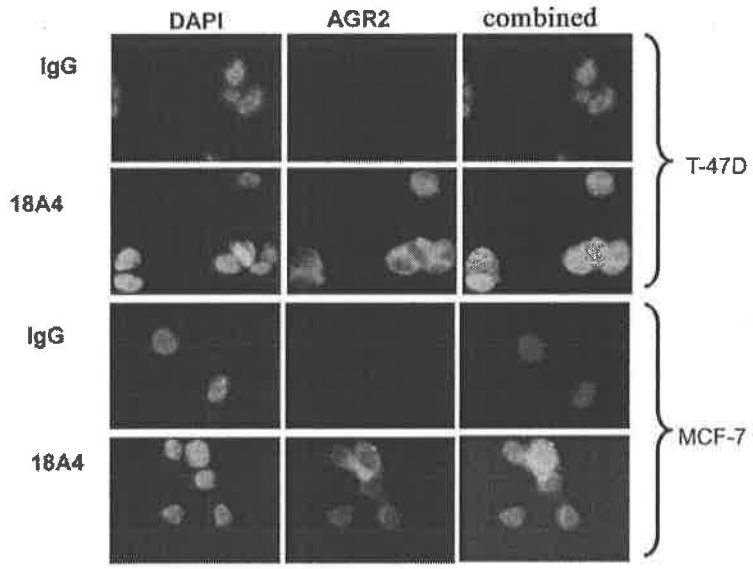


Figure 5A: Alignment of the light chain variable regions between the murine monoclonal antibody 18A4 and 18A4HU1

```
18A4HU1/VL      EIVLTQSPATLSLSPGERATLSCRASKSVSTSGYSYMHWYQQKPGQAPRLLIYLASNLESGIPARFSGSGSGTDFTLTISRLEPEDFAVYYCQHIRELPRTFGGGTKLEIK
human κ III     EIVLTQSPATLSLSPGERATLSCRASQSVSSS---YLAWYQQKPGQAPRLLIYGASSRATGIPARFSGSGSGTDFTLTISRLEPEDFAVYYCQ--------WTFGGGTKLEIK
18A4/VL         DIVLTQSPASLTVSLGQRATISCRASKSVSTSGYSYMHWYQRKPGQPPKLLIYLASNLESGVPARFSGSGSGTDFTLNIHPVEGEDAATYYCQHIRELPRTFGGGTKLEIK
                *       * ** * *  *    *  *    **  *   * *   * **** *          * *** *  * *         *
```

Figure 5B: Alignment of the heavy chain variable regions between the murine monoclonal antibody 18A4 and 18A4HU1

```
18A4HU1/VH      QVQLVQSGAEVKKPGASVKVSCKASGYTFTDYNMDWVRQAPGQGLEWIGDINPNYDTTSYNQKFKGKATLTVDKSTSTAYMELSSLRSEDTAVYYCARSMMGYGSPMDYWGQGTLVTVSS
human I         QVQLVQSGAEVKKPGASVKVSCKASGYTFTSYYMHWVRQAPGQGLEWMGIINPSGGSTSYAQKFQGRVTMTRDTSTSTVYMELSSLRSEDTAVYYCAR------Y------FDYWGQGTLVTVSS
18A4/VH         EVQLQQFGAELVKPGASVKISCKASAYTFTDYNMDWVKQSHGKSLEWIGDINPNYDTTSYNQKFKGKATLTVDKSSSTAYMELRSLTSEDTAVYYCARSMMGYGSPMDYWGQGTSVTVSS
                * * *  **      *   *  * * *  * ** **  * *  ****  *  * ** * * * * *  *  * *              *      *
```

Figure 6A: Structural comparison between the light chain variable region (V_L) of the murine monoclonal antibody 18A4 and the V_L of the humanized 18A4HU1 version

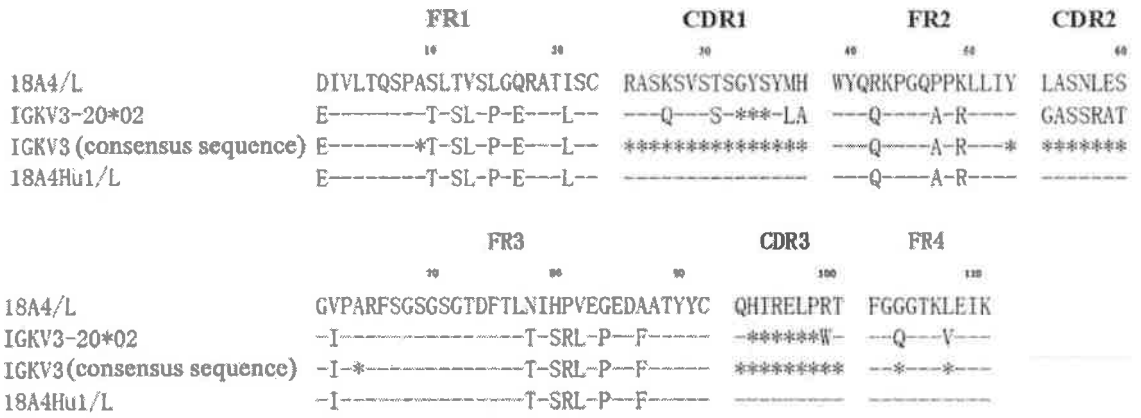


Figure 6B: Structural comparison between the heavy chain variable region (V_H) of the murine monoclonal antibody 18A4 and the V_H of the humanized 18A4U1 version

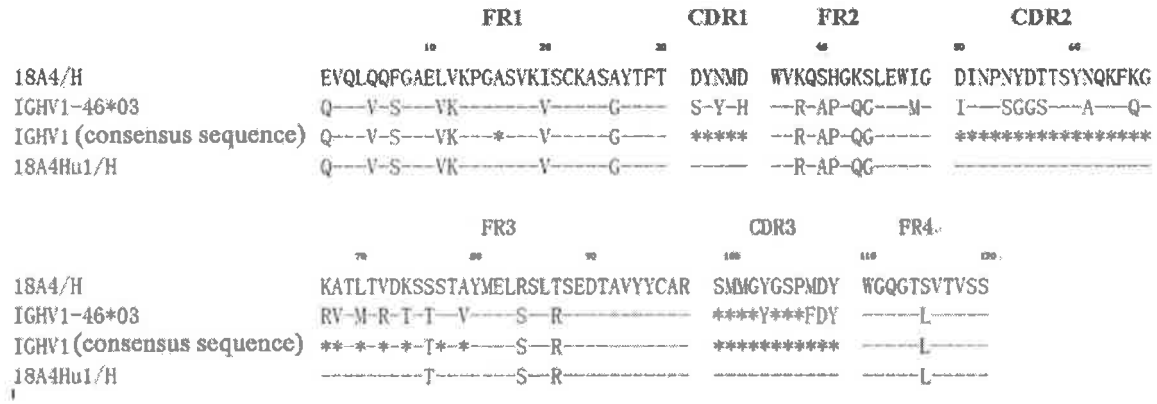


Figure 7: Diagram for the construction of the plasmid for expressing the intact antibody

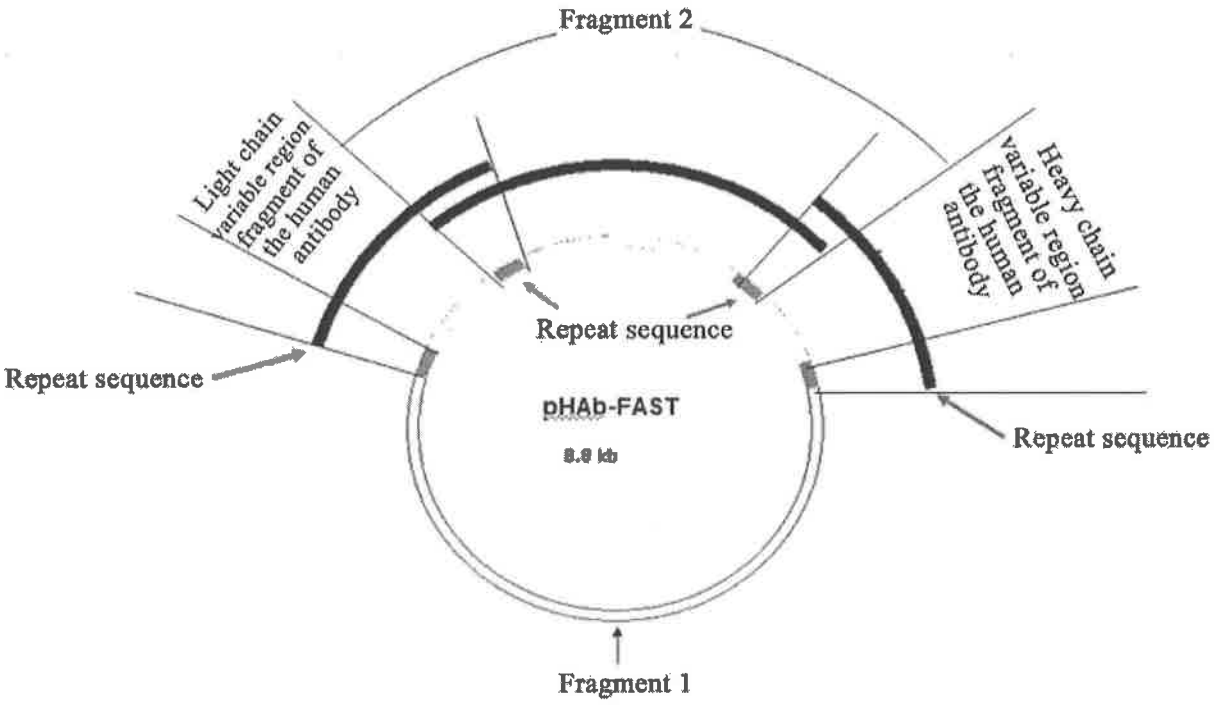


Figure 8: SDS-PAGE electrophoresis of the purified antibody

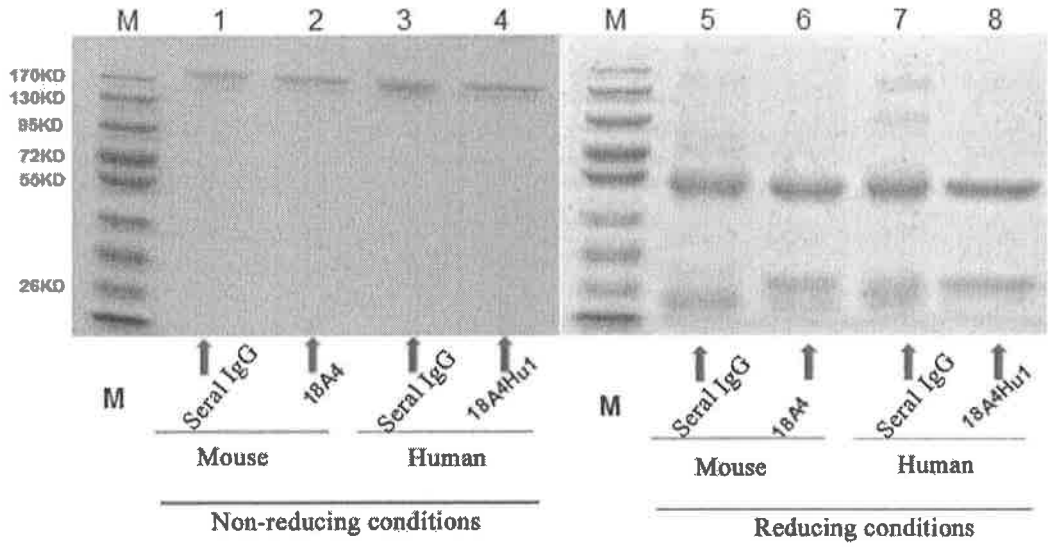


Figure 9: Experimental results for the antibody affinity assayed by a competitive ELISA

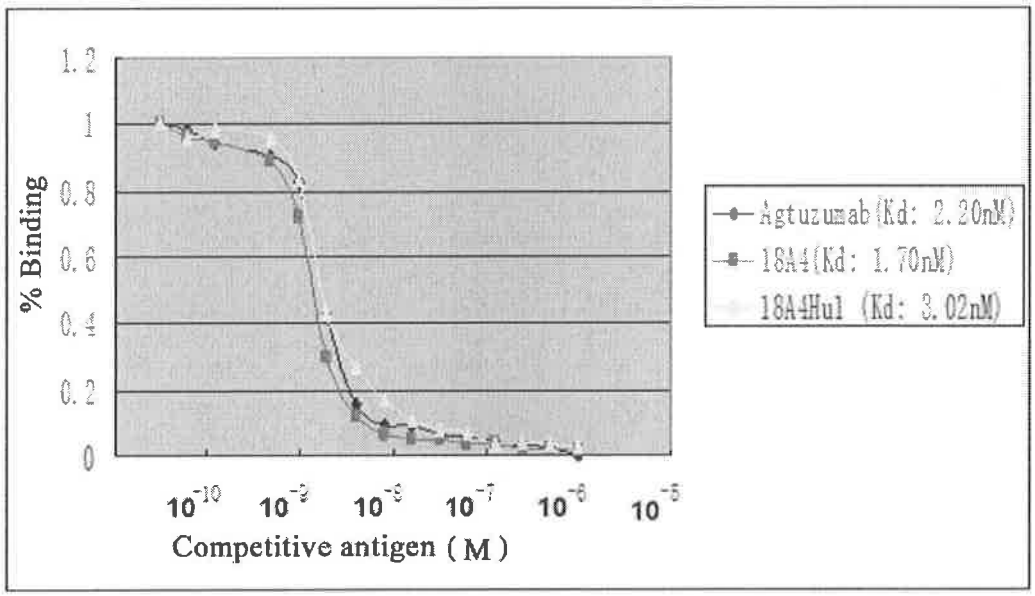


Figure 10: Alignment of the mutated positions in the humanized antibody variant and the change of the number of the potential T cell epitopes

Heavy chain mutation

Name	Mutation	HCDR2 and HFR2 T cell epitopes	Total T cell epitopes
18A4	YNQKFKGKATLTV	5+11	60
18A4Hu1	YNQKFKGKATLTV	5+11	44
18A4Hu2	YNQKFKGKVTMTV	2+6	36
18A4Hu3	YNQKFKGRVTMTV	2+5	35
Agtuzumab	YNQKFQGRVTMTV	0+5	33

Light chain mutation

Name	Mutation	LFR2 and LCDR2 T cell epitopes	Total T cell epitopes
18A4	LLIYLASNLES	5+3+14	41
18A4Hu1	LLIYLASNLES	5+3+14	26
18A4Hu4	LLIYLASSLET	5+2+1	12
18A4Hu5	LLIYLASSRET	2+2+1	9

Figure 11: Antigen binding curve of the humanized antibody variants

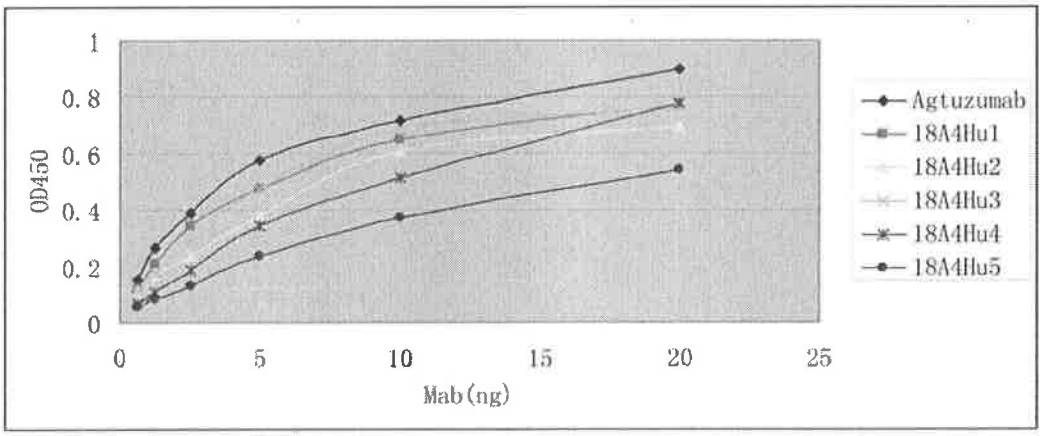


Figure 12: Identification of the species specificity of the humanized antibody Agtuzumab by western blot

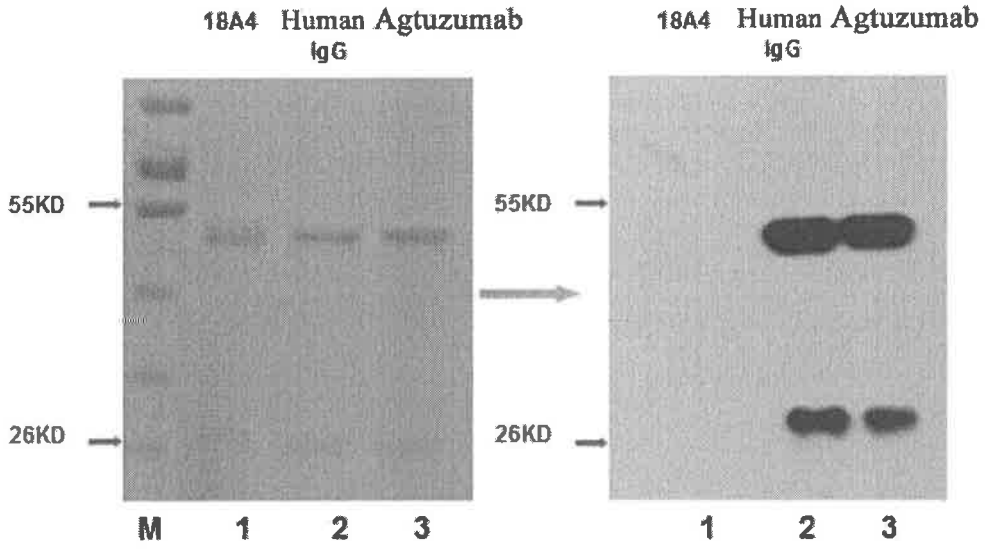


Figure 13: Detection of the antigen binding specificity of the humanized antibody Agtuzumab by western blot

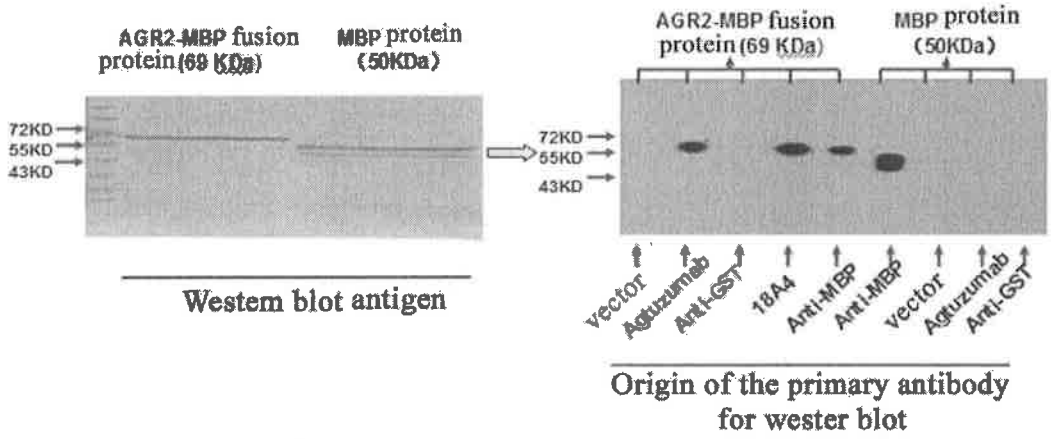


Figure 14: Detection of the binding specificity of the humanized antibody Agtuzumab to the antigens in the cell lysate by western blot

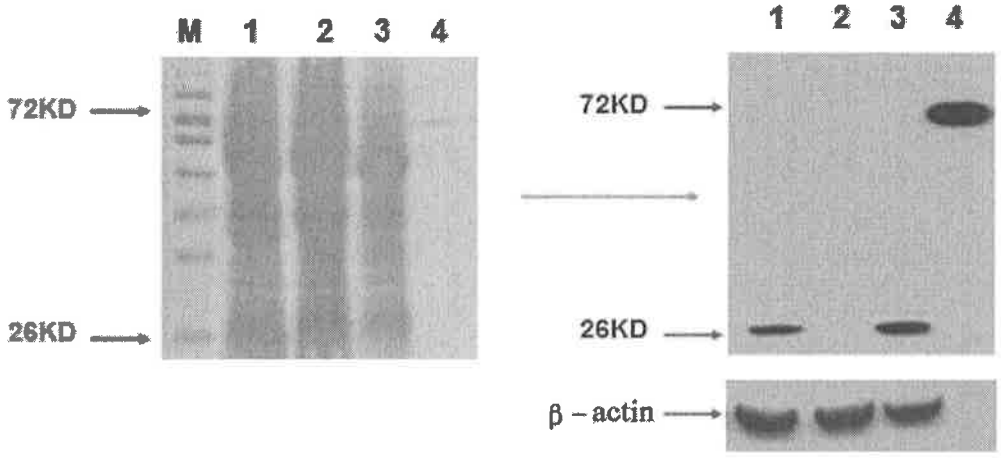


Figure 15: Detection of the ability of the humanized antibody Agtuzumab to bind to the natural AGR in the MCF7 cells by immunoprecipitation (IP)

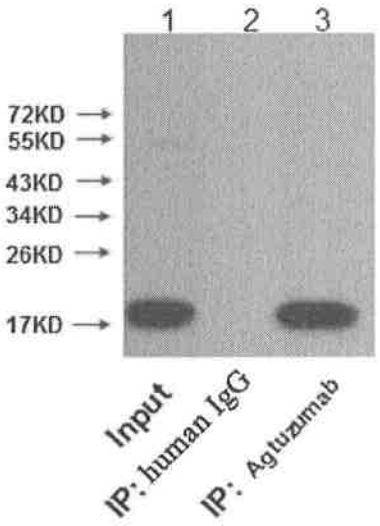


Figure 16: AGR2-MBP mutants generated by mutations according to the analysis of potential epitopes of AGR2

AGR2, From P71 to L175



Figure 17: Binding of the murine 18A4 and the humanized antibody Agtuzumab to the AGR2-MBP mutants

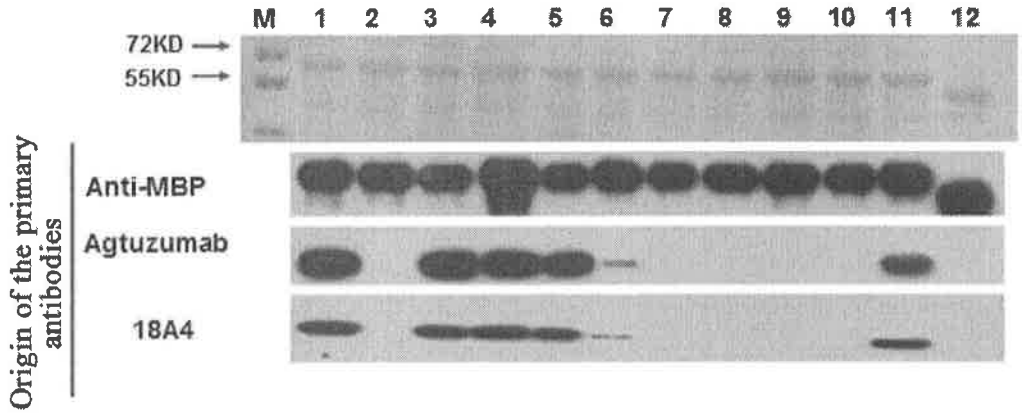
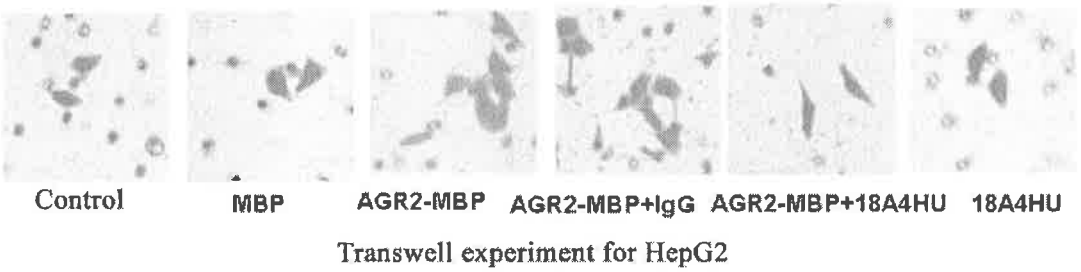


Figure 18: Detection of the ability of antibodies to inhibit the invasive metastasis of the liver cancer cell HepG2 in vitro by transwell experiments.



Transwell experiment for HepG2

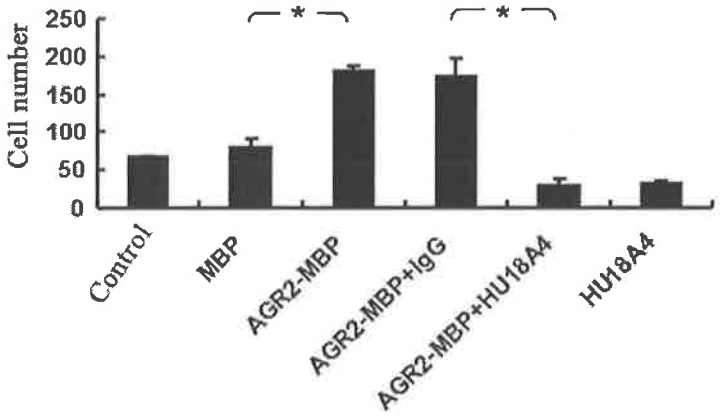


Figure 19: Detection of the ability of antibodies to inhibit the growth and migration of the breast cancer cells T47D and MCF 7 in vitro by MTT.

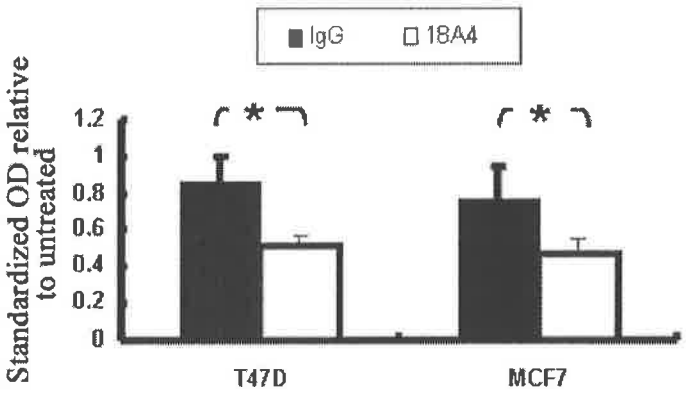
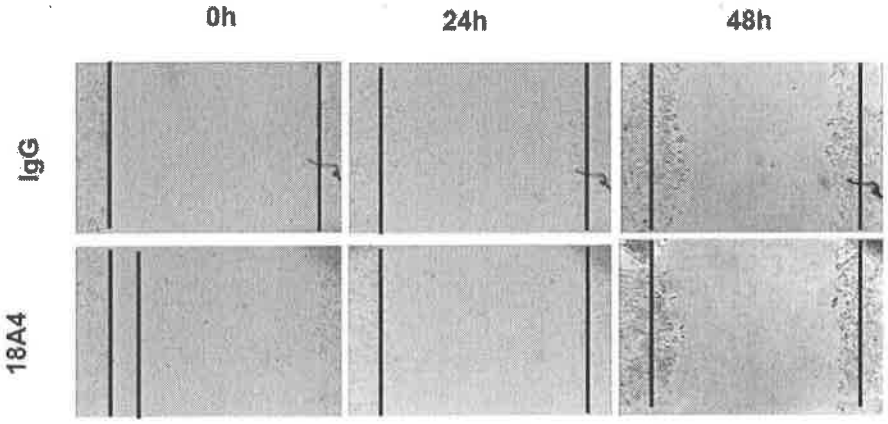


Figure 20:Detection of the ability of antibodies to inhibit the migration of the breast cancer cells T47D in vitro by wound healing assay.



Wound healing experiment for T47D

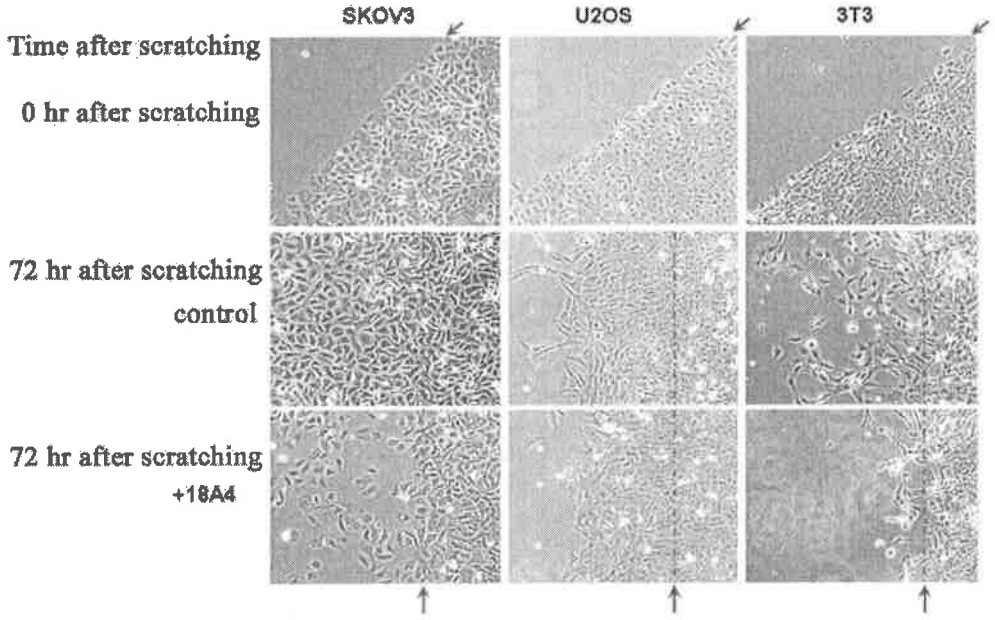
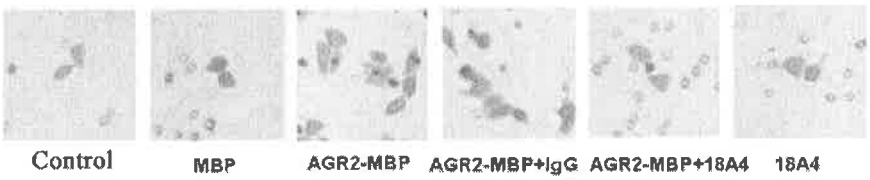
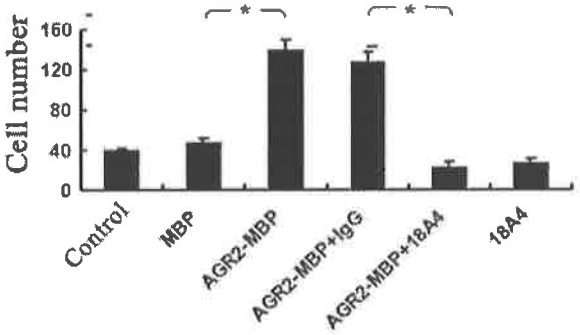
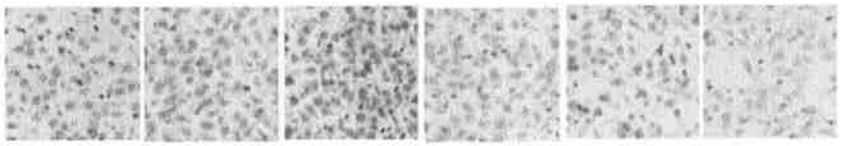


Figure 21: Detection of the ability of antibodies to inhibit the invasive metastasis of the liver cancer cell HepG2 in vitro by transwell experiments

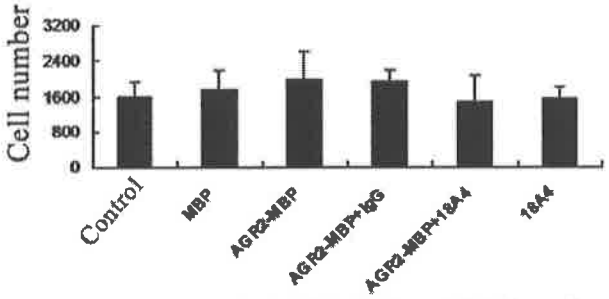


Transwell experiment for HepG2





Transwell experiment for SKOV3 (48h)



AGR2(25ug/ml), IgG(25ug/ml), 18A4(25ug/ml)

Figure 22:Detection of the ability of antibodies to inhibit the cell cycle of the breast cancer cells MCF-7 and T47D in vitro by cytometry

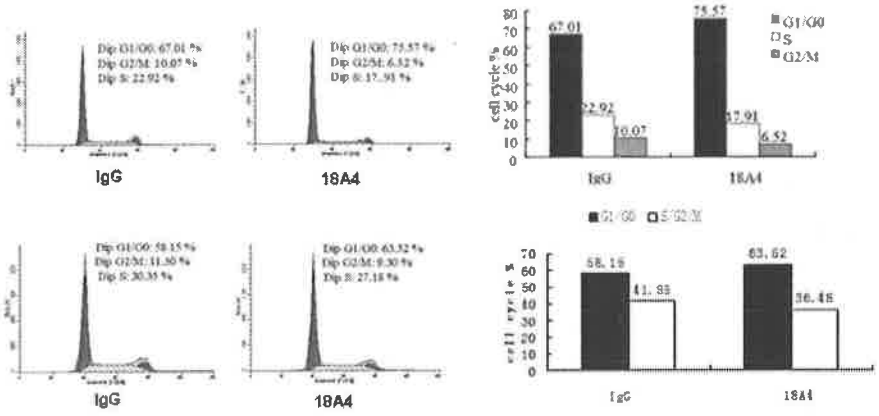


Figure 23: Confirmation of the binding of the antibodies to the AGR2 active site domain by western blot

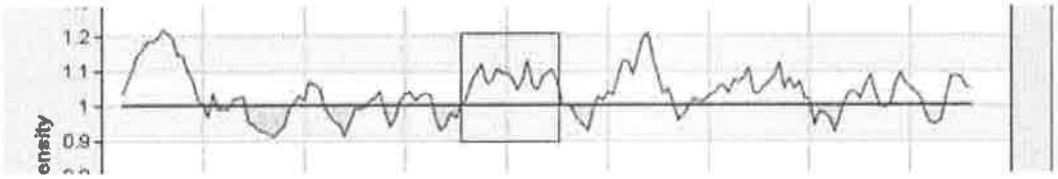


Figure 24: Confirmation of the binding of the antibodies to the AGR2 active site domain by western blot

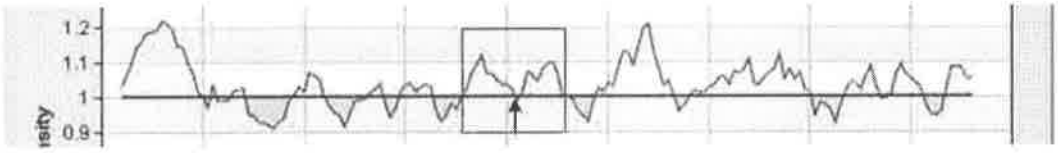


Figure 25: Confirmation of the binding of the antibodies to the AGR2 active site domain by western blot

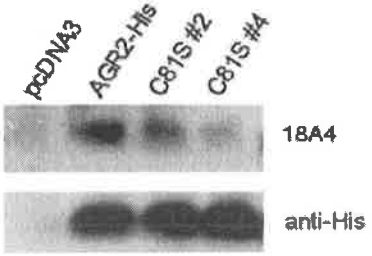


Figure 26: Tumor growth of animal

